FLOW DISTRIBUTION IN A SOLAR COLLECTOR PANEL WITH HORIZONTAL ABSORBER STRIPS

Fan, Jianhua; Shah, Louise Jivan; Furbo, Simon

Published in:
Solar Energy

Publication date:
2007

Document Version
Early version, also known as pre-print

FLOW DISTRIBUTION IN A SOLAR COLLECTOR PANEL WITH HORIZONTALLY INCLINDED ABSORBER STRIPS

Jianhua Fan*, Louise Jivan Shah, Simon Furbo

Department of Civil Engineering, Technical University of Denmark, Brovej, DK-2800 Kgs. Lyngby, Denmark

Abstract

The objective of this work is to theoretically and experimentally investigate the flow and temperature distribution in a solar collector panel with an absorber consisting of horizontally inclined strips. Fluid flow and heat transfer in the collector panel are studied by means of computational fluid dynamics (CFD) calculations. Further, experimental investigations of a 12.5 m² solar collector panel with 16 parallel connected horizontal fins are carried out. The flow distribution through the absorber is evaluated by means of temperature measurements on the backside of the absorber tubes. The measured temperatures are compared to the temperatures determined by the CFD model and there is a good similarity between the measured and calculated results.

Calculations with the CFD model elucidate the flow and temperature distribution in the collector. The influences of different operating conditions such as flow rate, properties of solar collector fluid, solar collector fluid inlet temperature and collector tilt angle are shown. The flow distribution through the absorber fins is uniform if high flow rates are used. By decreased flow rate and decreased content of glycol in the glycol/water mixture used as solar collector fluid, and by increased collector tilt and inlet temperature, the flow distribution gets worse resulting in an increased risk of boiling in the upper part of the collector panel.

Keywords: Solar collector; Flow distribution; Computational Fluid Dynamics (CFD); Buoyancy effects

1 Introduction

The thermal performance of flat-plate collectors is strongly related to the flow distribution through the absorber tubes (Duffie and Beckman, 1991). Investigations have conclusively shown that the collector efficiency decreases as the uniformity of flow distribution diminishes (Chiou, 1982). The more uniform the flow distribution, the higher collector efficiency. However, uniform flow distributions are not always present in solar collectors, as shown by Wang and Wu

* Corresponding author. ISES member Tel: +45-42251889 Fax: +45-45883282
Email addresse: jif@byg.dtu.dk (Jianhua Fan)

(1990), Shen (1992), Jones and Lior (1994), Weitbrecht et al. (2002) and Gunnewiek et al. (1996, 2002). Gunnewiek et al. investigated flow distribution in unglazed transpired plate collectors of large area both with (2002) and without the effect of wind (1996). The investigations were carried out by means of a commercial CFD code TASCFlow. It is shown that the flow of air through the collector surface is not uniformly distributed due to the buoyancy effects and that outflow of air may occur over part of the collector surface if suction flow is low enough. Shen (1992) studied the flow maldistribution in dividing and combining flow manifolds due to the effect of friction. Weitbrecht et al. (2002) investigated isothermal flow distribution in solar collectors with laminar flow conditions by means of LDV (laser Doppler velocimetry) measurements and numerical analysis. Jones and Lior (1994) presented the numerical investigations of flow distribution in solar collectors consisting of two horizontal manifolds connected by a number of parallel riser tubes without considering thermal effects. Wang and Wu (1990) presented flow distribution in solar collectors with thermal effects such as longitudinal heat conduction and buoyancy. Both collectors with U type configuration and collectors with Z type configuration were investigated. Although there is no contradictory from physical point of view, the flow distribution pattern of Z type collectors found by Jones and Lior does not match the results of Wang and Wu. The flow pattern found by Jones and Lior is increasing with the increase of the distance along the inlet manifold (Fig. 6 and 7 of Jones and Lior, 1994), while the flow pattern found by Wang and Wu is first decreasing with the increase of branch number and then increasing with the increase of branch number (Fig. 5 of Wang and Wu, 1990). This type of behaviour is not the result of buoyancy, but of a greater role of inertia in the manifolds (vs. friction). For frictionally dominant manifolds, the riser flow rates tend to be monotonic with distance along the inlet manifold. As the number of branches are increased and/or distance between the branches reduced, the pressure distributions in the manifolds tends to become dominated by inertial pressure changes in the branch regions. The riser flow distribution then behaves in a non-monotonic manner, where there is a region of flow starved risers away from the ends of the collector.

The aim of this work is to theoretically and experimentally investigate the flow and temperature distribution in a solar collector panel with an absorber consisting of horizontally inclined fins. Fluid flow and heat transfer in the collector panel are studied by means of computational fluid dynamics (CFD) calculations. A simplified model is built, where the geometry including the manifolds and the quadrangular absorber tubes are fully modelled, while the existence of the fins is represented by a heat flux into the absorber tube walls. The model includes heat transfer and buoyancy effects. The influences of the flow and temperature distributions by different operation conditions such as flow rate, properties of solar collector fluid, solar collector fluid inlet temperature and collector tilt angle are investigated, while the influence of the flow distribution on collector thermal efficiency is not considered.

Measurements are carried out with a 12.5 m² solar collector panel with 16 parallel connected horizontal fins. The flow distribution through the absorber is evaluated by means of temperature measurements on the backside of the absorber tubes. The measurements are carried out for different flow rates, temperature levels and solar irradiances. The measurements are compared to the results of the CFD calculations.

2 Experimental work

Steady state measurements are carried out with a 12.5 m^2 flat-plate solar collector panel from Arcon Solvarme A/S. The solar collector is a high temperature HTU solar collector designed for medium and large solar heating systems. The collector has also with advantage been used recently in small solar heating systems. Fig. 1 shows the design of the HTU solar collector. The collector consists of two manifolds (one dividing and one combining manifold) with a diameter of 0.0256 m and 16 horizontally inclined absorber tubes in a "U" type configuration (Vejen et al. 2004), see Fig. 2. The quadrangular absorber tubes have a hydraulic diameter of 0.0067 m.

A propylene glycol/water mixture is used as the solar collector fluid. Properties of the mixture and their dependences on temperature for 40% (weight %) glycol solution are shown as follows (Furbo, 1997):

Density, [kg/m^3] $\rho = 1042 - 0.479 * T - 0.00185 * T^2$

Dynamic viscosity, [kg/(ms)] $\mu = 0.0016 * (\frac{T + 273.15}{333.15})^{-8}$

Specific heat, [J/(kgK)] $C_p = 3721 + 1.629 * T + 0.0101 * T^2$

Thermal conductivity, [W/(mK)] $\lambda = 0.419 + 2.032 \times 10^{-4} * T$

where T is fluid temperature, [°C].

The solar collector fluid is circulated through the collector panel by a pump. The circulating flow rate, in the range of 2.5-25.0 l/min, is measured using a QEC type Clorius flow meter. The flow distribution through the absorber tubes is evaluated by fluid temperature distribution just before the fluid enters the combining manifold. Copper-constantan thermo couples (type TT) are attached to the backside of the absorber tubes and used for the temperature measurements. The positions of the measurement points are schematically shown in Fig. 2 as circles on the left side. Since the absorber tube wall has a higher temperature than the fluid inside, small corrections are made to the temperature measurements to get the fluid temperatures. The corrections are determined based on the difference between the measured solar collector fluid outlet temperature and the mean of the measured absorber tube wall temperatures, see the following approximated equation:

$$T_{fluid,i} = T_{wall,i} - \left(\frac{\sum_{i=1}^{16} T_{wall,i} \cdot Q_i}{Q_0} - T_{outlet}\right) \quad (1)$$

where $T_{\mathrm{fluid,i}}$ is the fluid temperature in *i* th tube, ºC; $T_{\mathrm{wall,\,i}}$ is the temperature of the *i*th tube wall, ºC; T_{outlet} is the outlet temperature from the collector, ºC; Q_{i} is the volume flow rate through the *i* th tube, l/min, while Q_0 is the overall volume flow rate for all the tubes, l/min. The fluid velocities in the absorber tubes used in the equation are obtained from CFD simulation. Since the correction is small, the error introduced by this method will not significantly influence the credibility of the determination of the fluid temperature.

Solar irradiance on the collector panel is measured using a pyranometer type CM11 from Kipp & Zonen. The data collection and control program IMPVIEW is used to measure the inlet flow rate and temperature, ambient temperature and solar irradiance as constant values during the test period.

The accuracy of the measuring equipment is given in Table 1.

3 Numerical investigations

The flow distribution through the absorber tubes is investigated numerically with CFD. A simplified model is built using the CFD code Fluent 6.1 (Fluent Inc., 2003), where the whole fluid passage including both the combining and the dividing manifolds and the 16 quadrangular absorber tubes are fully modelled, while the existence of the fins is represented by a heat flux into the absorber tube walls, assuming uniform energy generation in the tube wall. This representation of an absorber plate by a heat flux into the tube wall is not the same physics as heat transfer from a thin absorber plate into a tube. Since incorporation of the 16 absorber plates into the model is complicated and the calculated temperatures of the present model are in a fairly good agreement with temperatures from the experiments, the approximation is acceptable. The heat flux is determined by the following equation:

$$\text{heat flux} = W_{fin} \cdot \eta_0 \cdot G \quad (2)$$

where W_{fin} is the width of the fin (m) and η_0 is the start efficiency of the solar collector efficiency expression. A measured start efficiency of 0.83 is used. G is the solar irradiance, W/m^2.

The heat loss from the absorber strips is strongly related to the air flow conditions inside and around the collector panel and influenced by weather conditions like ambient air and sky temperature. Consequently the heat loss varies in a complicated way for different operation conditions and the heat loss from the absorber strips is difficult to determine. In this study, the collector casing is not included in the model. The heat loss from the absorber strips is assumed to be transferred only by means of convection which can be determined by a convective heat loss coefficient and the ambient

air temperature. A solar collector calculation program, SOLEFF, developed by Rasmussen and Svendsen (1996) is used to determine the heat loss coefficient, which is used as input for the CFD simulations. The heat loss coefficient is adjusted in such a way that the collector efficiency calculated with the CFD program is equal to the measured collector efficiency. Since the heat loss from the manifolds is only a small part of heat loss from the collector, it is not considered. Since for most conditions the fluid flow in the tubes and in the manifolds falls in the laminar region and very few cases fall in the transition region, laminar flow model was used in the CFD calculation. A uniform velocity inlet boundary condition is used for the inlet flow to the collector and a pressure outlet boundary condition is used for the outlet flow from the collector. Steady state simulations were performed with Boussinesq approximation for buoyancy modelling. The PRESTO and second order upwind method were used respectively for the discretization of the pressure and the momentum equations. The SIMPLE algorithm is used to treat the pressure-velocity coupling (Fluent Inc., 2003). The simulations start from a zero velocity with solution of energy equation disabled in order to get an initial velocity field. Then the simulations continue with heat transfer and buoyancy effects considered. The solution is considered convergent if the scaled residual for the continuity equation, the momentum equations and the energy equation are less than 1.0×10^{-4}, 1.0×10^{-4} and 1.0×10^{-7} respectively. One typical simulation takes approximately 12 hours for a computer with 3 GHz CPU frequency and 1G memory.

Due to the large difference in the dimension of absorber tube length (5.790 m) and tube hydraulic diameter (0.0067 m), a very fine grid distribution is needed in the cross section of the tube. Fig. 3 shows grid distribution for the tubes and manifolds. Positions of View plane A is schematically shown in Fig. 2. View A shows grid distribution at the tubes and manifold. View B and View C show grid setup at the cross-section of the manifold and the quadrangular tube respectively. Since flow distribution through the tubes is of interest, the mesh density of the tubes (unstructured, hexahedron, 4.2E-9 m^3/cell on average) is almost 2 times higher than that of the manifolds (unstructured, hexahedron/tetrahedron, 1.1E-8 m^3/cell on average), which results in about 1.4 million mesh cells for the whole model. A mesh dependent study of the CFD model shows that an increase of the mesh density of the manifolds does not influence the prediction of calculated efficiency significantly. If the mesh cells of the 16 absorber tubes were increased from 1.1 million to 1.9 million by increasing the number of mesh nodes in the length of the tubes and the mesh density in the cross section of the tubes, the refined mesh will only slightly improve the accuracy of the predicted collector efficiency, but it takes much more computer memory and computational time to solve the flow control equations, therefore a mesh scheme with 1.4 million mesh cells altogether is used.

4 Results

The fluid flow through the *i*th tube (counted from the top) is characterized by a parameter β_i, defined as follows.

$$\beta_i = \frac{Q_i}{Q_0} \tag{3}$$

where Q_i is the volume flow rate through the *i*th tube, while Q_0 is the overall volume flow rate for all the tubes.

For an ideal, uniform flow distribution through 16 tubes, β_i equals to 1/16. However, this is not always the case in the solar collector. Instead, strong deviations from uniform flow distribution have been observed in this work as well as in previous investigations of other collectors. A relative flow non-uniformity parameter Φ is introduced to quantify the flow maldistribution. Φ is defined as

$$\Phi = \sqrt{\frac{\sum_{i=1}^{16}(\beta_i - 1/16)^2}{16}} * \left(1/16\right)^{-1} * 100\% \tag{4}$$

From its definition, it can be seen that the relative flow non-uniformity parameter is similar to the root-mean-square or standard deviation generally used in the statistical treatment of experiment data, except it is divided by the mean value (1/16).

The ratio between the Grashof number and Re^2 is introduced to quantify the importance of buoyancy forces in the fluid flow in the collector panel (see equation 5). When this ratio exceeds unity, strong buoyancy contributions to the flow are expected. Conversely, if it is very small, buoyancy forces may be ignored in the investigation (Fluent Inc., 2003).

$$\frac{Gr}{\mathrm{Re}^2} = \frac{g \cdot \sin\theta \cdot \beta \cdot \Delta T \cdot L}{U^2} \tag{5}$$

where g is gravity force, m/s^2; θ is the tilt angle of the collector panel, °; ΔT is characteristic temperature difference, K. The temperature difference between solar collector fluid inlet and outlet temperature is used. β is the thermal expansion coefficient, 1/K; L is characteristic length, m, which is defined as height of the collector panel. U is the averaged fluid velocity in the absorber tubes, m/s.

The flow and temperature distribution through the 16 parallel absorber tubes are investigated under different operation conditions. The parameters investigated are inlet flow rates: 2.5, 4.0, 5.0, 10.0 and 25.0 l/min, solar collector fluid inlet temperatures: 20°C, 60°C and 80°C, collector tilt angles: 10°, 40° and 70° and with and without buoyancy effects.

4.1 Isothermal flow

Investigations show that without thermal effects flow distribution through the tubes is subject to the influence of the collector configuration parameters such as the ratio of tube diameter D_i to manifold diameter D_0, the number of tubes and the length of the tubes (Jones and Lior, 1994). Fig. 4 presents CFD simulations of isothermal flow distribution and its

comparison with Jones and Lior's data. The CFD simulation was carried out with the temperature of the collector constantly at 60ºC. It should be mentioned that the *Re* value indicated in the figure is the Reynolds number of the inlet flow which is much larger than the Reynolds number of flow in the manifold and in the absorber tubes. From the figure, it can be seen that the flow rate through the tubes tends to decrease from top tubes to bottom tubes. When the inlet flow rate increases, the flow distribution gets worse. The relative flow non-uniformity parameter Φ increases from 2.8% to 6.4% when the inlet flow rate increase from 2.5 l/min to 25.0 l/min. Jones and Lior's data show the same tendency, but a little more evenly distributed (Φ =1.4%). This disagreement is most likely due to the difference in collector design and operation parameters. The solar collector used in this study has a D_i to D_0 ratio of 0.26 and 16 tubes 5.96 m in length, while it was a collector with a D_i to D_0 ratio of 0.25 and 16 tubes 1.83 m in length in Jones and Lior's investigations. Moreover, the collector fluid is propylene glycol/water mixture in this work, while it was water with an inlet flow rate of 1.89 l/min in Jones and Lior's work.

4.2 Inlet flow rate

The analysis above may not be valid if buoyancy effects are taken into consideration. CFD simulations were carried out to show how the flow distribution will be influenced by the buoyancy effects. A collector panel with a tilt angle of 40° is used in the investigations. The collector is assumed to operate at a constant ambient temperature of 20°C and to be heated with a solar irradiance of 800 W/m^2. The influence of solar collector volume flow rate on the flow and temperature distribution of the collector panel is shown in Fig. 5.

Comparing Fig. 5 with Fig. 4, it can be seen that for higher flow rates such as 10.0 l/min and 25.0 l/min, the flow distribution almost remain unchanged. But for lower flow rates such as 2.5 l/min, 4.0 l/min and 5.0 l/min, the buoyancy effects are significant. The buoyancy driving force tends to circulate clockwise inside the collector panel, thus decreasing the flow rate in the upper absorber tubes and increasing the flow rate in the lower absorber tubes. As shown in Fig. 5 (A), the distribution curves for flow rates of 2.5 l/min, 4.0 l/min and 5.0 l/min are different from the curves in Fig. 4. The lower the flow rate, the stronger the influence of the buoyancy effects will be. For flow rate less than 5.0 l/min, the buoyancy force is so strong that the tendency of flow distribution curve changes. For isothermal flow, the flow rate maximizes at the top and decreases from top to bottom tube, while it is the other way around when the flow rate is lower than 5.0 l/min. This means that the collector fluid in the upper tubes will stay a longer time in the tubes and reach a relatively higher temperature, while the fluid in the lower tubes will reach a relatively lower temperature. The temperature distribution of the collector fluid at the end of the absorber tubes is shown in Fig. 5 (B). Here, T_i stands for fluid temperature of the *i*th tube just before the fluid enters the combining manifold and T_{mean} is the mass flow rate

weighted average of all T_i. When the flow rate decreases from 25.0 l/min all the way to 2.5 l/min, the tilt of the temperature distribution curve will increase.

Fig. 6 presents results of thermal experiments and its comparison with CFD simulations. It is shown that for a flow rate of 24.9 l/min, the fluid temperatures at the end of all the absorber tubes are almost the same, with a variation of no more than 2 K. When the flow rate drops from 10.4 l/min to 5.2 l/min and 3.9 l/min, the temperature difference will increase to 7 K, 13 K and 16 K respectively. For an even smaller flow rate such as 1.9 l/min, there is a strong increase of the temperature difference to about 58 K. Even though the collector panel is heated by a relatively weaker solar irradiance 616 W/m^2 and has a lower inlet temperature 30ºC, the fluid temperature at the end of the top tube rises above 109ºC. This temperature is higher than the boiling point, 103.9ºC for a 40% propylene glycol/water mixture under the pressure of 1 atm. Strong oscillations, observed in the measurements, in the flow rate and outlet temperature series indicate the existence of boiling inside the collector panel when the inlet flow rate is 1.9 l/min.

The risk of boiling will increase if the inlet temperature increases. Fig. 7 shows CFD calculated temperatures of the collector panel with a tilt angle of 40º when the collector fluid enters the panel at 2.5 l/min and 60ºC, and is heated by a solar irradiance of 800 W/m^2. The fluid temperature in the dividing manifold is shown to be the same as the inlet temperature. As the fluid flows along the tube, the collector fluid gains heat and its temperature rises. The fluid temperature at the end of the top 4 absorber tubes rises above the boiling point under the pressure of 1 atm.

Boiling in the collector panel may cause problems such as steam blockage which will create poor heat transfer and decrease collector thermal performance, and flow oscillations which will initiate vibration and pulse like steam release. Further, the strips with the boiling fluid might expand so much that strips might get in physical contact with the glass cover of the collector. At worst it may cause physical damage on the collector and acidification of the collector fluid which will lead to corrosion of the collector. For the 40° tilted collector investigated in this work, the flow rate should be no less than 4.0 l/min (0.32 kg/min per m^2 solar collector) in order to avoid boiling if the solar irradiance is 800W/m^2 and the solar collector fluid inlet temperature is 60°C.

Further, the comparison between CFD simulation and thermal measurement is shown in Fig. 6. There is a good agreement for flow rates such as 5.2 l/min and 10.4 l/min. However, for a lower flow rate of 1.9 l/min, there are large differences between measured and calculated temperatures. This indicates that the method is not accurate enough. Following points should be considered in order to improve the method:

- The air temperature and its distribution inside the collector panel have a significant influence on flow and temperature distribution through the tubes. The air gap temperature is obtained theoretically from SOLEFF. Further measurements of the air gap temperatures will be necessary for validation of the model.

- The solar collector is simplified with only fluid passage (manifolds and absorber tubes) modelled. A detailed description of the whole collector might improve the accuracy of the calculations.

Despite these points, the method of analysing the flow and temperature distribution through the absorber tubes seems promising. Therefore, the influences of operation parameters such as inlet flow rate, the collector tilt, the inlet temperature and the solar collector fluid on the flow distribution are investigated by the method and described in the following.

4.3 Collector tilt angle

The buoyancy driving force takes effect due to the gravity force, so the larger the collector tilt, the stronger the influence of buoyancy effects will be. For a solar collector fluid inlet temperature of 60°C, Fig. 8 presents calculated flow and temperature distributions for collectors of different tilt angles. The figure clearly shows that for a flow rate of 2.5 l/min the flow distribution gets worse with increasing tilt angle. The relative non-uniformity parameter increases by about 4 times when the tilt angle increases from 10° to 70°. Accordingly the temperature difference between the coldest and warmest tube just before the fluid enters the combining manifold increases from 5.6 K to 77 K.

For a flow rate of 10.0 l/min, the influence of tilt angle on flow and temperature distribution is small, simply because the buoyancy driving force is comparably smaller than the friction of fluid flow through the collector tubes and thus does not have a dominant influence.

4.4 Solar collector fluid inlet temperature

The influence of the inlet temperature on flow and temperature distribution is investigated and shown in Fig. 9. For a flow rate of 2.5 l/min, the relatively flow non-uniformity parameter is 10.8% and 18.7% for solar collector fluid inlet temperature of 20°C and 60°C respectively. For a flow rate of 10.0 l/min, the relative flow non-uniformity parameter increases from 3.4% to 5.2% when the solar collector fluid inlet temperature rise from 20°C to 80°C. For higher temperatures, the collector fluid (propylene glycol/water mixture) has a larger thermal expansion coefficient and thus a stronger buoyancy driving force. Moreover, the fluid viscosity will decrease so the significance of buoyancy driving force increases. The possibility of boiling will increase with the increase of solar collector fluid inlet temperature. For a flow rate of 2.5 l/min, boiling will definitely occur under the pressure of 1 atm if the inlet temperature increases from 20°C to 60°C, while for a flow rate of 10.0 l/min, boiling is more likely to occur if the inlet temperature increases above 90°C.

4.5 Properties of Solar collector fluid

The flow distribution through the tubes will get worse if water or a less concentrated aqueous glycol solution is used as solar collector fluid. Figure 10 shows the influence of fluid properties on flow and temperature distributions if the solar

collector fluid enters the collector at 20°C and is circulated through the collector panel at 2.5 l/min. It can be seen that the maximum fluid temperature difference between the top and the bottom strip just before the fluid enters the combining manifolds is 28.6K, when a 40% glycol solution is used as solar collector fluid. If a 20% glycol solution or water is used as solar collector fluid, the maximum fluid temperature difference increases to 37.6K and 47.7K respectively. Correspondingly the relative flow nonuniformity parameter increases from 10.8% to 19.2% and 27.5%. This is mainly due to the fact that if the glycol concentration of the solar collector fluid decreases the fluid viscosity will decrease and the significance of buoyancy effects will increase resulting in a more unevenly distributed fluid flow through the absorber tubes.

5 Discussion

The above investigations are summarized and the influences of different parameters are analyzed which includes solar collector volume flow rates (2.5, 4.0, 5.0, 10.0, 25.0 l/min), inlet temperatures (20, 60, 80°C), tilt angles (10, 40, 70°) and solar collector fluid properties (pure water, 20% and 40% glycol/water mixture). The ratio between Grashof number and Re^2 is introduced to quantify the importance of buoyancy forces in the fluid flow in the collector panel and to analyze the influences of different parameters on the flow distribution. The plot of flow nonuniformity versus the Gr/Re^2 value is given in Fig. 11.

There are three forces dominating the flow distribution in the collector panel: The pressure drop in the absorber tubes, the inertial and frictional pressure changes in the manifolds and the buoyancy effects. For a high collector fluid volume flow rate of 25.0 l/min and 10.0 l/min, the Gr/Re^2 value fall in the range of 0.069-1.6 which means that the inertial force in the tubes is significant while the buoyancy force is not strong and can be neglected. The flow distribution is governed by the combination of pressure drop in the absorber tubes and the inertial and frictional pressure changes in the manifolds. The flow pattern for 25.0 and 10.0 l/min is the same as for an isothermal flow, where the flow rate decreases from top tubes to bottom tubes of the U type collector.

With a decrease of solar collector volume flow rate to 4.0 l/min, the Gr/Re^2 value increases to 16. The buoyancy force begins to dominate the flow distribution due to the cold dividing manifold to the right and the warm combining manifold to the left. The buoyancy driving force tends to circulate clockwise inside the collector panel, thus decreasing the flow rate in the upper absorber tubes and increasing the flow rate in the lower absorber tubes. The buoyancy force is so strong that the pattern of flow distribution change. The flow rate through the absorber tubes increases from the top tubes to the bottom tubes. With a decrease of the solar collector fluid volume flow rate to 2.5 l/min, the Gr/Re^2 value falls in the range of 17 to 99 which means that the buoyancy effects has a significant influence on the flow distribution through the

absorber tubes, resulting in a relatively high flow nonuniformtiy. From the definition, it can be seen that an increase of tilt angle, thermal expansion coefficient and a decrease of fluid velocity will increase the Gr/Re^2 value, therefore the influence of buoyancy force on the flow distribution will increase. Fig. 11 shows that flow nonuniformity Φ will increase by 1.3 and 3.1 times with an increase of the tilt angle from 10° (case 6) to 40° (case 4) and 70° (case 1) respectively. For a tilt angle of 40°, the flow nonuniformity decreases with the increase of Gr/Re^2. This tendency is different from the tendency of tilt angle due to the fact that fluid viscosity of the solar collector fluid, which is not included in Gr/Re^2, has a strong influence on the flow distribution. For a tilt angle of 40°, the flow nonuniformity increases with the increase of inlet fluid temperature and with the decrease of glycol concentration. With the increase of inlet fluid temperature from 20°C (case 5) to 60°C (case 4), the temperature difference between the outlet fluid and inlet fluid temperature will decrease so the Gr/Re^2 value decreases. With the increase of mean fluid temperature, the fluid viscosity will decrease from 2.6×10^{-3} to 1.0×10^{-3} kg/(m·s) resulting in a decreased pressure drop in the absorber tubes. Therefore the relative significance of buoyancy effects will increase which will worsen the flow maldistribution of the U type collector. With a decrease of glycol concentration from 40% (case 5) to 20% (case 3) and to 0% (case 2), the thermal expansion coefficient β will decrease so the Gr/Re^2 value will decrease. Since the viscosity of the fluid will decrease by 50% and 75% respectively with the decrease of glycol concentration from 40% to 20% and from 40% to 0%, the pressure loss in the absorber tubes will decrease with an increase of the significance of buoyancy effects, resulting in a worse flow distribution.

It can be concluded that for a low flow rate of 2.5 l/min (corresponding to 0.2 l/min per m^2 solar collector), flow distribution through the strips are not uniform. The flow nonuniformity is strongly influenced by the dominance of buoyancy forces to inertial forces and is therefore in a complicated way influenced by the solar collector fluid properties e.g. viscosity and thermal expansion coefficient as well as by the collector geometry e.g. the length of manifold and the operation conditions e.g. solar collector fluid volume flow rate, inlet fluid temperature and collector tilt angle.

6 Results

A numerical and experimental investigation of the flow and temperature distribution in a 12.5 m² solar collector panel with an absorber consisting of 16 parallel connected horizontal fins is performed. Numerically, the flow distribution through the absorber tubes is investigated with CFD. Experimentally, the flow distribution through the absorber is evaluated by means of temperature measurements on the backside of the absorber tubes.

Comparisons between CFD simulations and the thermal measurements show that for high flow rates, there is a good degree of similarity between measured and calculated fluid temperatures. However, for low flow rates there are large

differences between measured and calculated temperatures. This disagreement is most likely due to oversimplification of the collector model and lack of knowledge of the air flow conditions inside the collector panel. These points should be considered in further studies in order to improve the method.

The flow distribution is investigated for different flow rates, fluids temperatures of inlet flow and collector tilt angles. The results show that the buoyancy driving force will decrease the flow rate in the upper tubes and increase the flow rate in the bottom tubes. The lower the flow rate, the stronger the influence of buoyancy effects will be. When the inlet flow rate is 2.5 l/min, the collector tilt angle and temperature of inlet flow will have a significant influence on the flow and temperature distribution through the absorber tubes: The flow distribution gets dramatically worse with the increase of tilt angle and inlet temperature. The flow nonuniformity will increase if water or a less concentrated aqueous glycol solution is used as solar collector fluid. However, this influence is much less significant for a high flow rate, simply because the buoyancy driving force does not have a dominant influence for a flow rate of 10.0 l/min.

Thus, if the flow rate is too small, the solar collector fluid inlet temperature is too high and the collector tilt is too large, non-uniform flow distribution caused by buoyancy forces will occur in collectors with parallel horizontal fins. This will result in a decreased collector efficiency and an increased risk of boiling of the solar collector fluid and an attention to this problem is therefore of great importance. Consequently, it is recommended to improve the methods used in this study in order to improve our knowledge on the thermal behaviour of the collectors.

Nomenclature

C_p	specific heat [J/(kg·K)]
D_i	Tube diameter [m]
D_0	Manifold diameter [m]
g	gravity force, [m/s^2]
G	Solar irradiance, [W/m^2]
L	characteristic length, [l]
Q_i	volume flow rate though the *i*th tube [m^3/s]
Q_0	overall volume flow rate for all the tubes [m^3/s]
T_i	fluid temperature at the end of *i*th tube [°C]
T_{mean}	mass flow rate weighted average of T_i for all the tubes [°C]
U	fluid velocity in absorber tubes, [m/s]
W_{fin}	fin width, [m].

ΔT	temperature difference, [K]
β	thermal expansion coefficient, [1/K]
β_i	ratio of Q_i to Q_0 [-]
θ	slope of the collector panel, [º]
η_0	start efficiency in solar collector efficiency expression, [-]
λ	thermal conductivity [W/(m·K)]
μ	fluid dynamic viscosity [kg/(m·s)]
ρ	fluid density [kg/m^3]
Φ	relative flow non-uniformity parameter [-]

References

Chiou J. P., 1982. The effect of nonuniform fluid flow distribution on the thermal performance of solar collector, Solar Energy 29 (6) 487-502.

Duffie J. A., Beckman W. A., 1991. "Solar Engineering of Thermal Processes", 2nd edition, John Wiley & Sons, New York, pp. 320-322.

Fluent Inc., 2003. Fluent release 6.1, 10 Cavendish Court, Lebanon, NH 03766-1442 USA.

Furbo S., 1997. "Varmelagre til solvarmeanlæg", Institut for Bygninger og Energi, Technical University of Denmark, pp. 22-23.

Gunnewiek, L. H., Brundrett E., Hollands K.G.T., 1996. Flow distribution in unglazed transpired plate solar air heaters of large area, Solar Energy 58 (4-6), 227-237.

Gunnewiek, L.H., Hollands K.G.T., Brundrett E., 2002. Effect of wind on flow distribution in unglazed transpired plate collectors, Solar Energy, 72 (4), 317-325.

Jones G. F., Lior N. L., 1994. Flow distribution in manifolded solar collectors with negligible buoyancy effects, Solar Energy 52 (3), 289-300.

Rasmussen P. B. Svendsen S., 1996. "SolEff Program til beregning af solfangeres effektivitet". Brugervejledning og generel programdokumentation, Thermal Insulation Laboratory, Technical University of Denmark.

Shen P. I., 1992. The effect of friction on flow distribution in dividing and combining flow manifolds, ASME J. Fluids Eng. 114, 121-123.

Vejen, N. K., Furbo S., Shah L.J., 2004. Development of 12.5m^2 solar collector panel for solar heating plants, Solar Energy Materials and Solar cells, 44, 205-223.

Wang X. A., Wu L. G., 1990. Analysis and performance of flat-plate solar collector arrays, Solar Energy 45 (2), 71-78.

Weitbrecht V., Lehmann D., Richter A., 2002. Flow distribution in solar collectors with laminar flow conditions, Solar Energy 73 (6), 433-441.

Tables

Clorius Flow meter	± 1 %
Kipp & Zonen pyranometer	± 2 %
Thermocouples Type TT	± 0.5 K

Table 1: Accuracy of measuring equipment.

Figure captions

Fig. 1: Design of the investigated “U” type HTU solar collector.

Fig. 2: A schematic illustration of the “U” type configuration of the HTU flat plate solar collector.

Fig. 3: Grid setup for the manifold and the quadrangular absorber tube of the HTU solar collector.

Fig. 4: Flow rate distribution of the “U” type collector for isothermal flow. *Re* is the Reynolds number of the inlet flow.

Fig. 5: Volume flow rate and fluid temperature distributions in the strips for different solar collector fluid volume flow rates.

Fig. 6: Measured and calculated fluid temperature at 30 cm from the combining manifold.

Fig. 7: Temperature (°C) contour at the middle plane of the collector for a flow rate of 2.5 l/min, a solar collector fluid inlet temperature of 60°C and a solar irradiance of 800 W/m^2.

Fig. 8: Volume flow rate and fluid temperature distributions in the strips for different collector tilt angles and solar collector fluid volume flow rates. The inlet temperature is 60°C.

Fig. 9: Volume flow rate and fluid temperature distributions in the strips for different solar collector fluid inlet temperatures.

Fig. 10: Volume flow rate and fluid temperature distributions in the strips for different solar collector fluids.

Fig. 11: Plot of flow nonuniformity parameter Φ (%) of the U type collector versus Gr/Re^2 for different solar collector volume flow rates.

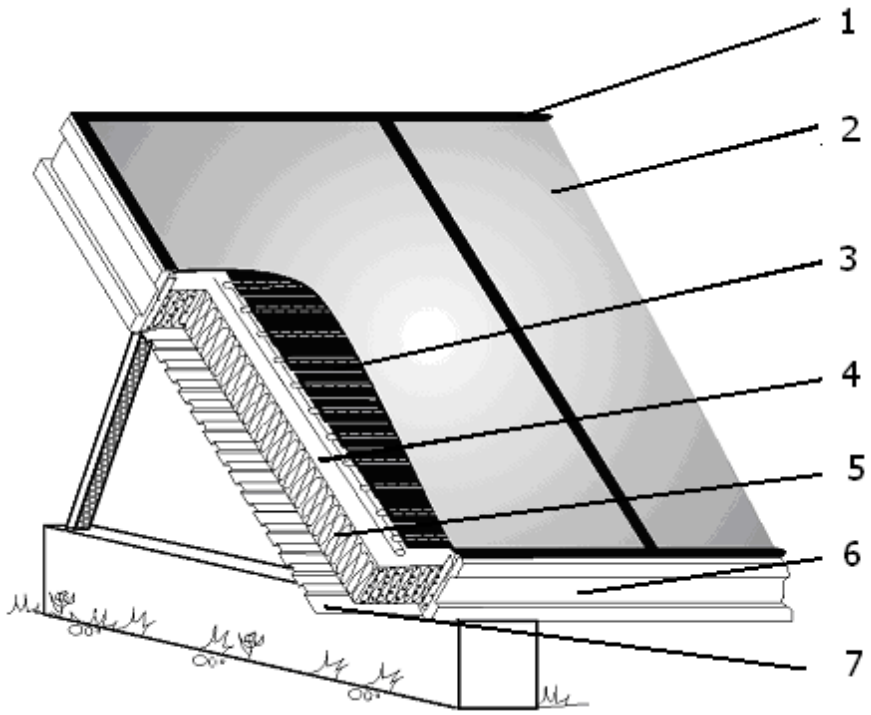

1 Glass framing: Top and bottom mouldings made of EPDM-rubber.
2 Glass: 4 mm, non-iron, and non-breakable glass with a fitted back side.
3 Absorber: Copper tube/aluminium plate with selective surface.
4 Vapour and diffusion trap: Aluminium foil.
5 Insulation: 75 mm glass wool.
6 Sill profile: Extruding aluminium profiles.
7 The back side: 0.5 mm treated aluminium sheet.

Fig. 1: Design of the investigated “U” type HTU solar collector.

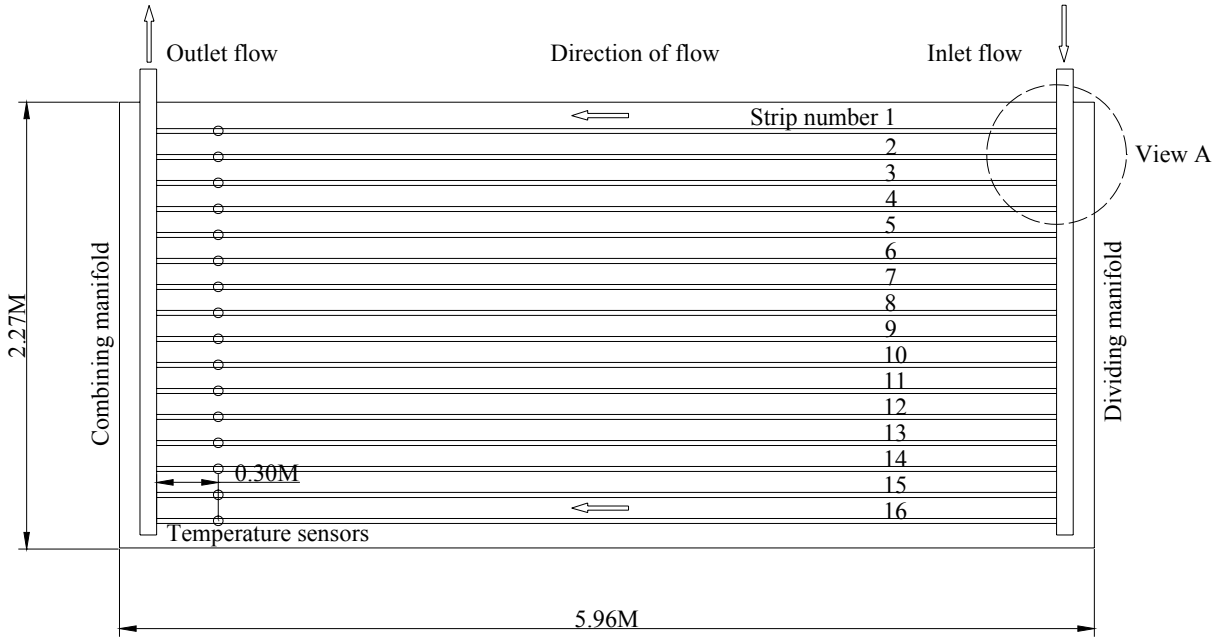

Fig. 2: A schematic illustration of the "U" type configuration of the HTU flat plate solar collector.

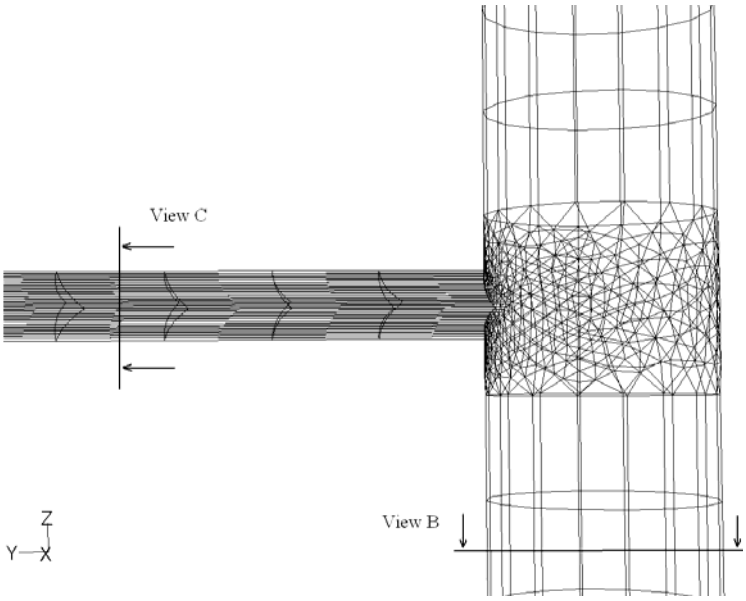

View A

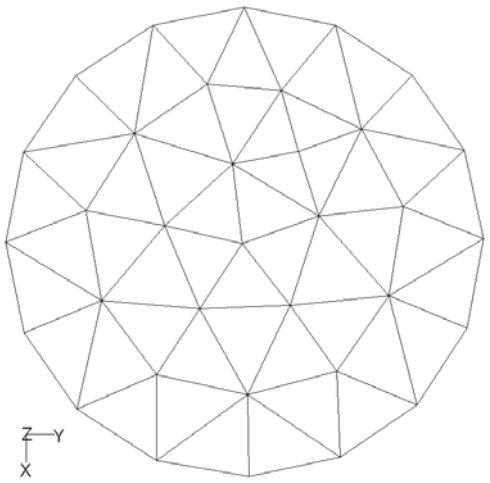

View B

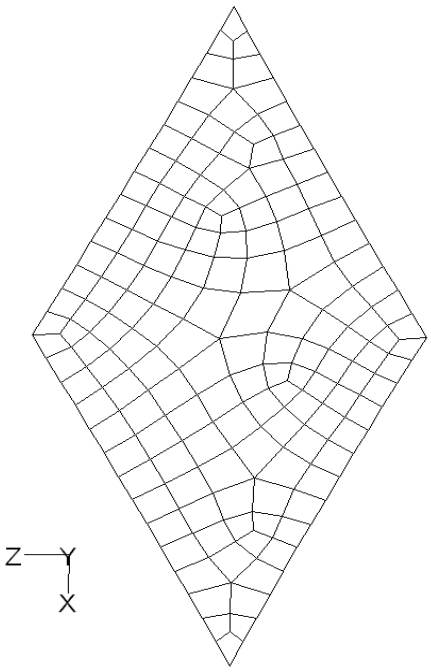

View C

Fig. 3: Grid setup for the manifold and the quadrangular absorber tube of the HTU solar collector.

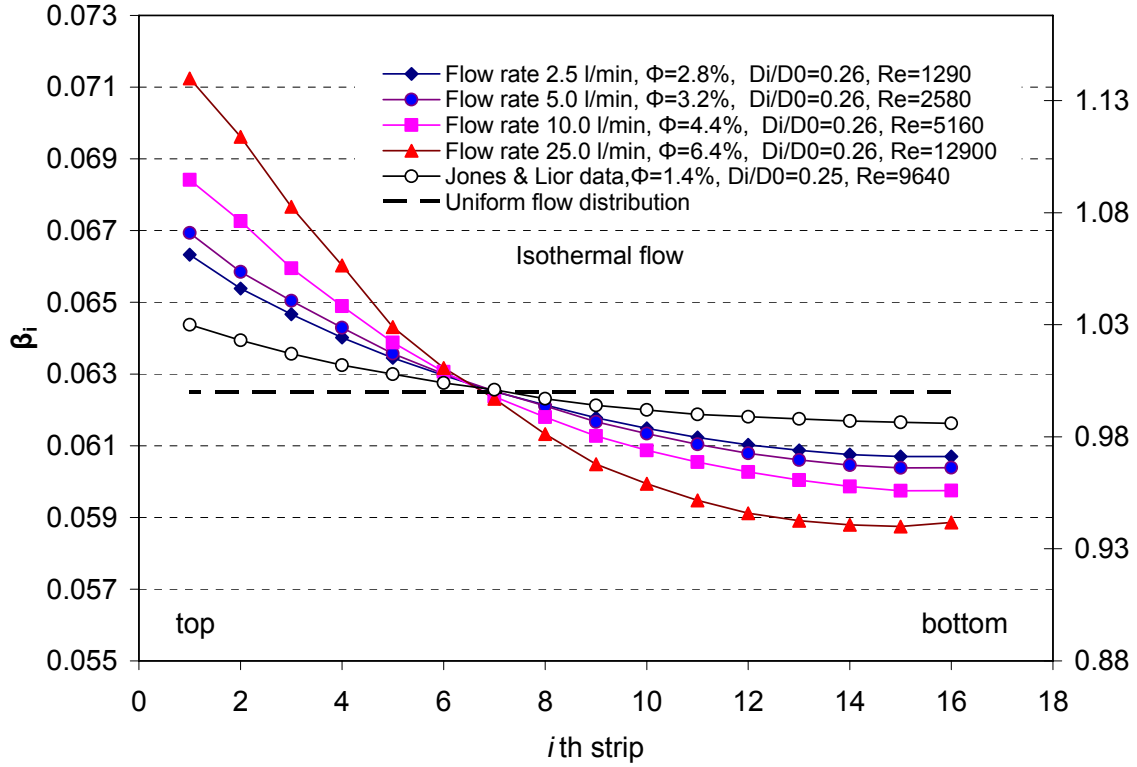

Fig. 4: Flow rate distribution of the "U" type collector for isothermal flow. *Re* is the Reynolds number of the inlet flow.

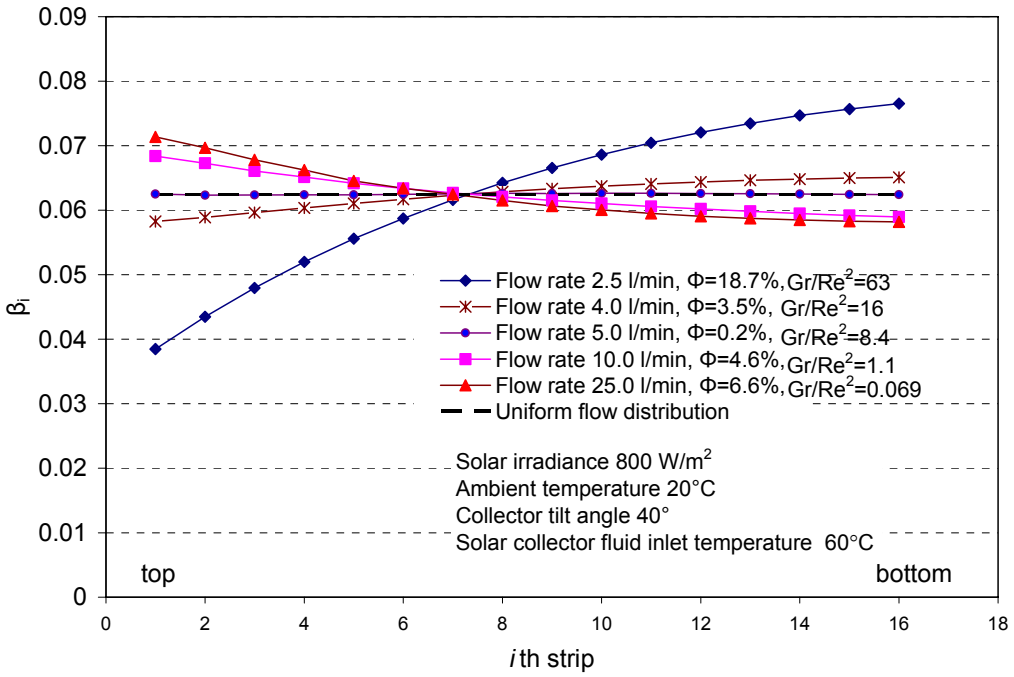

(A) Flow distribution

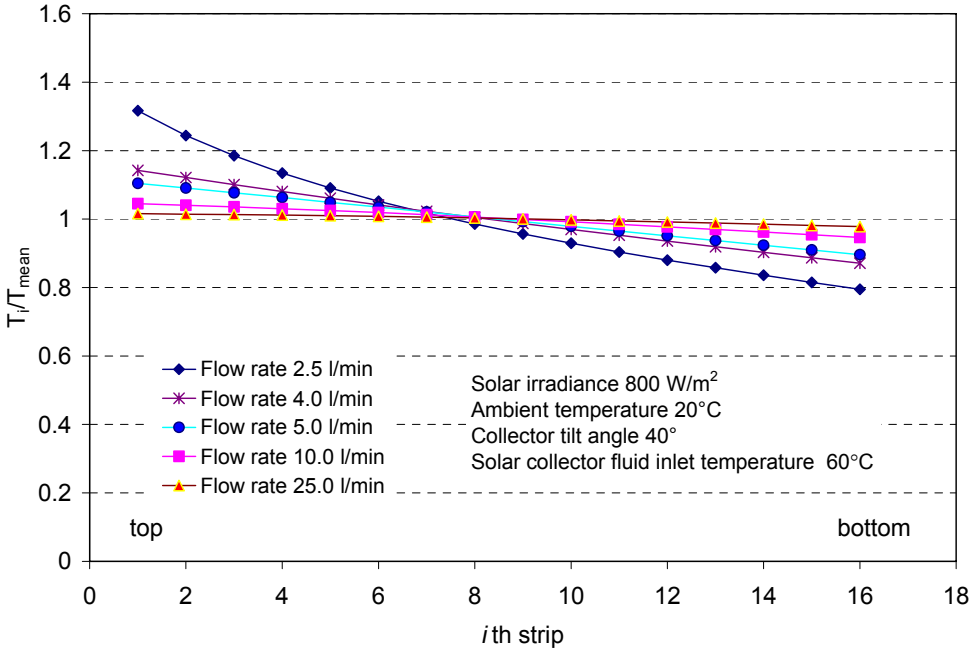

(B) Temperature distribution

Fig. 5: Volume flow rate and fluid temperature distributions in the strips for different solar collector fluid volume flow rates.

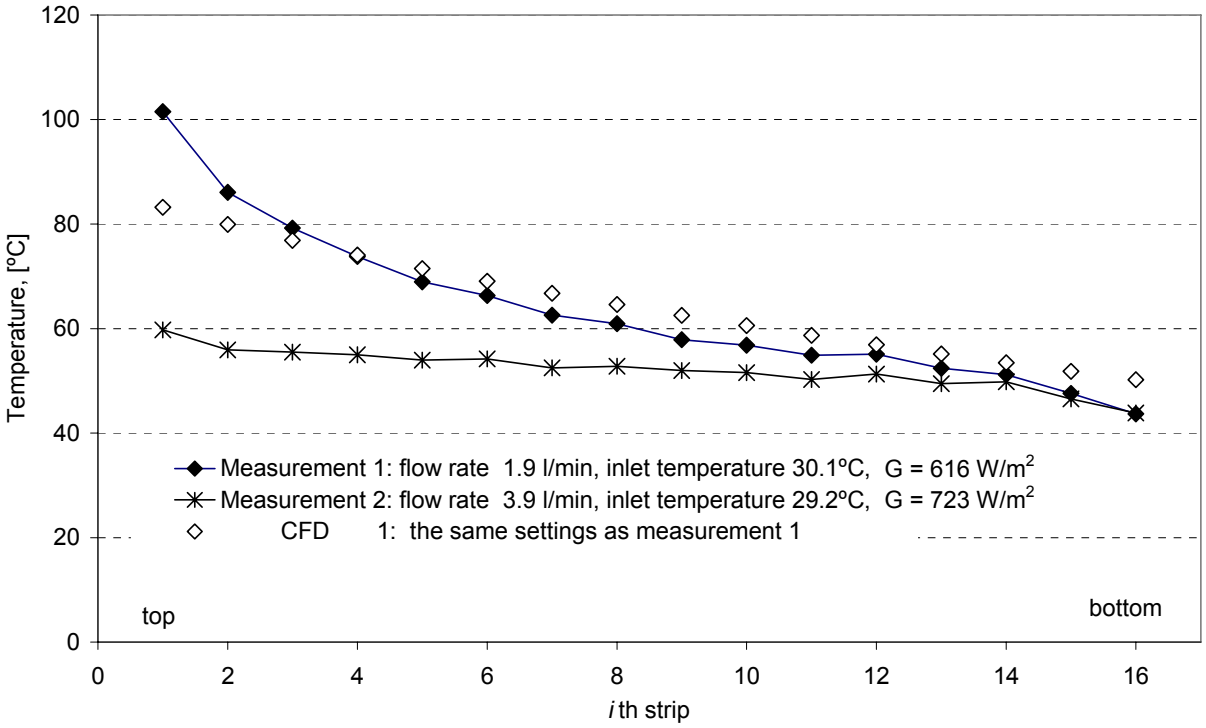

(A) Flow rates less than 4 l/min

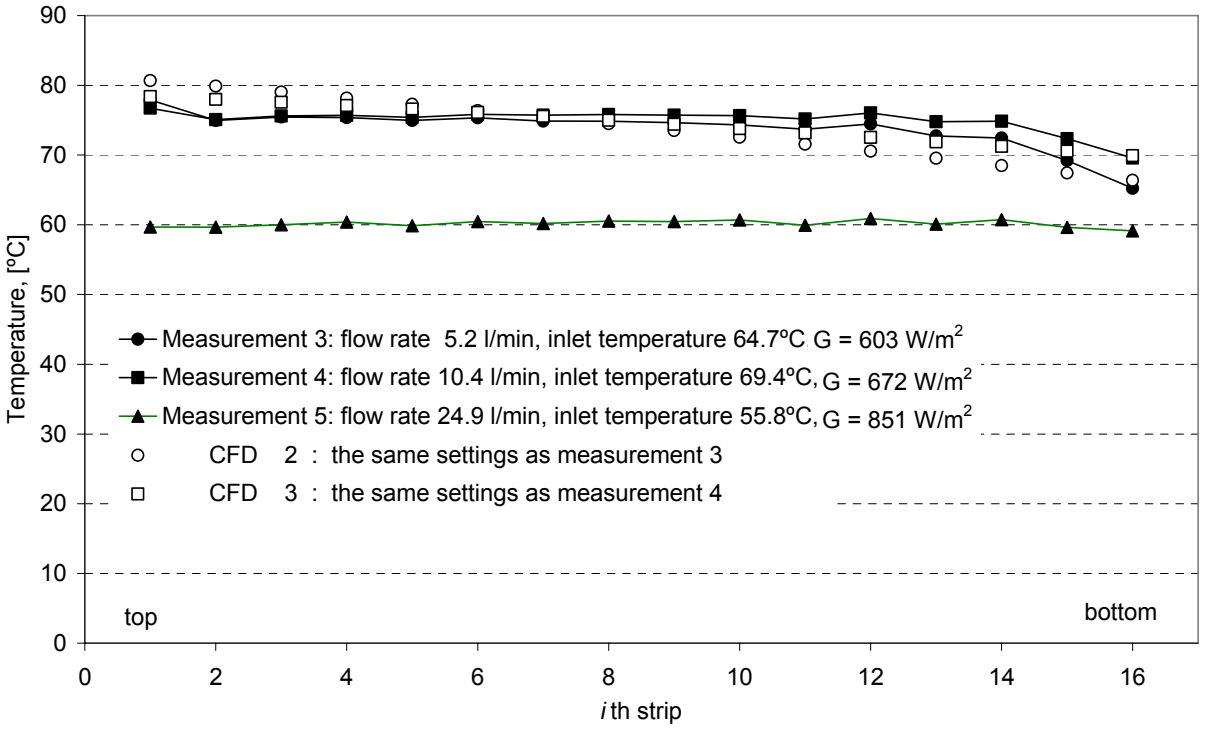

(B) Flow rates greater than 4 l/min

Fig. 6: Measured and calculated fluid temperature at 30 cm from the combining manifold.

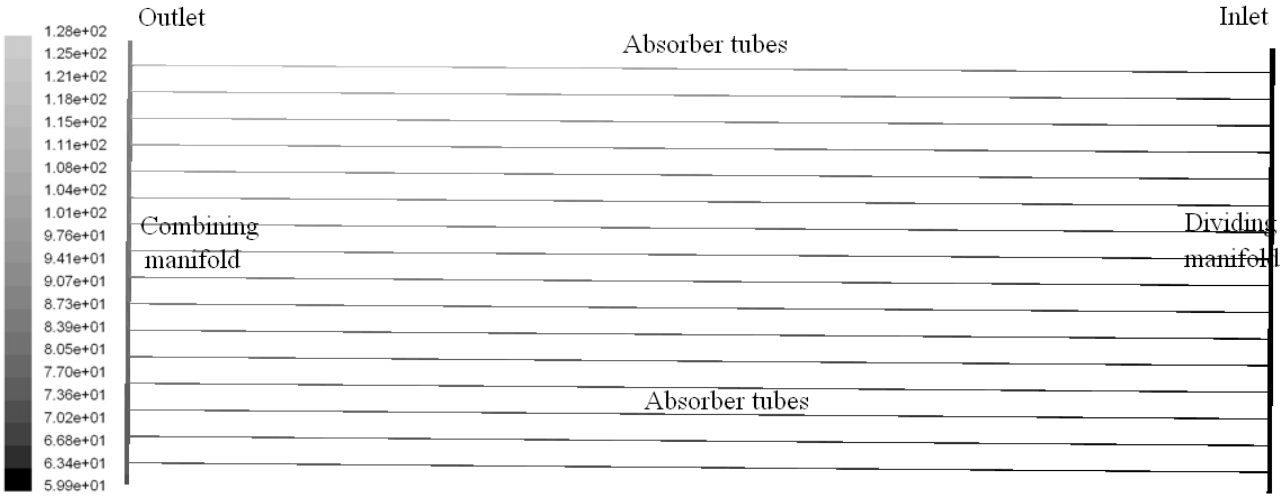

Fig. 7: Temperature (°C) contour at the middle plane of the collector for a flow rate of 2.5 l/min, a solar collector fluid inlet temperature of 60°C and a solar irradiance of 800 W/m^2.

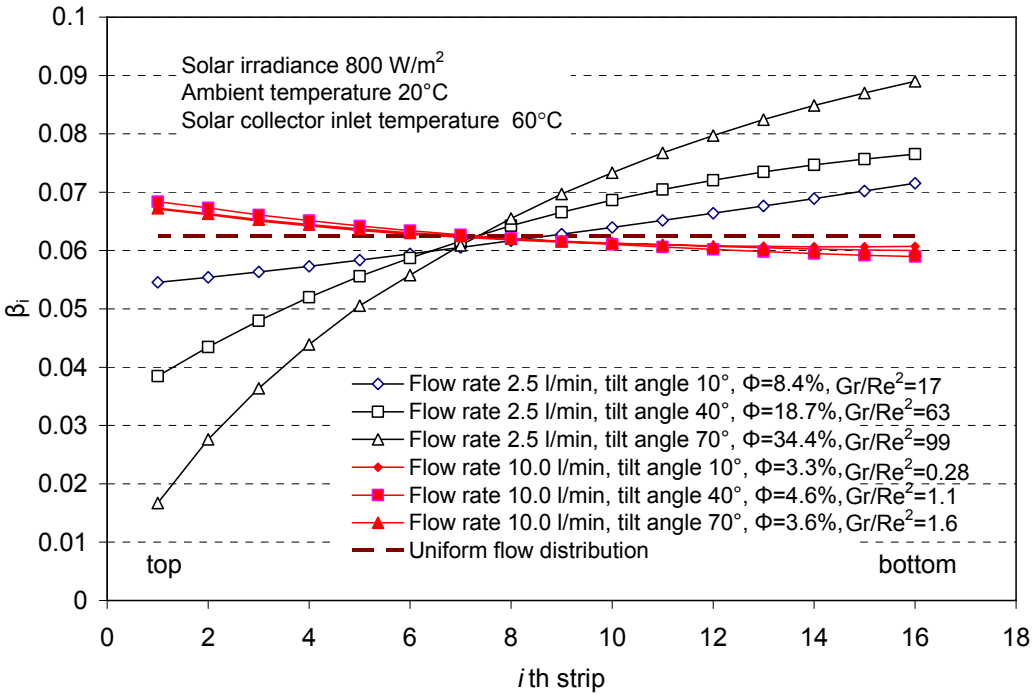

(A) Flow distribution

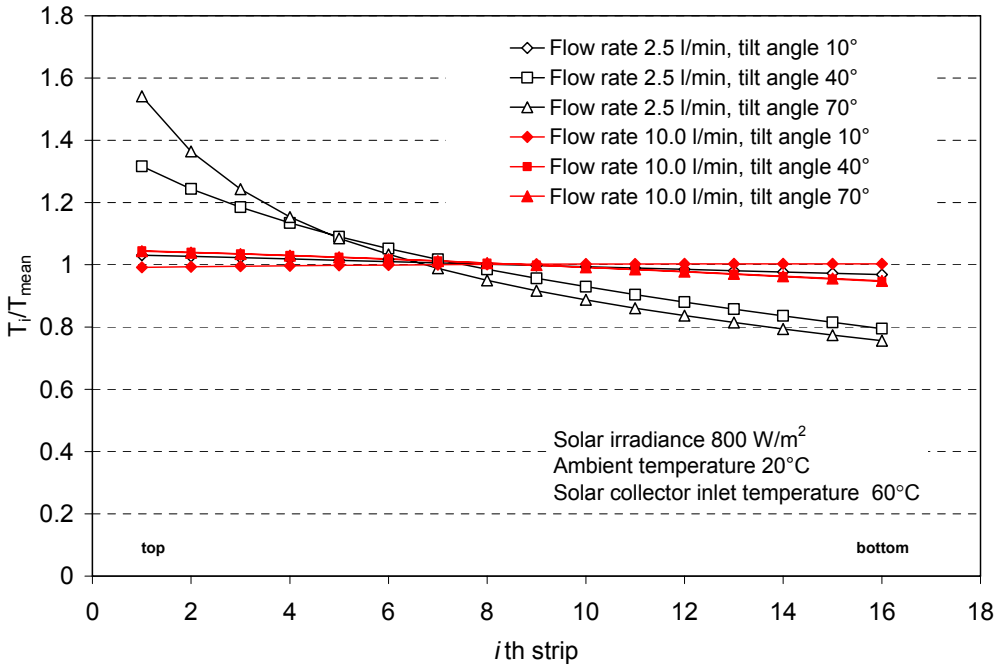

(B) Temperature distribution

Fig. 8: Volume flow rate and fluid temperature distributions in the strips for different collector tilt angles and solar collector fluid volume flow rates. The inlet temperature is 60°C.

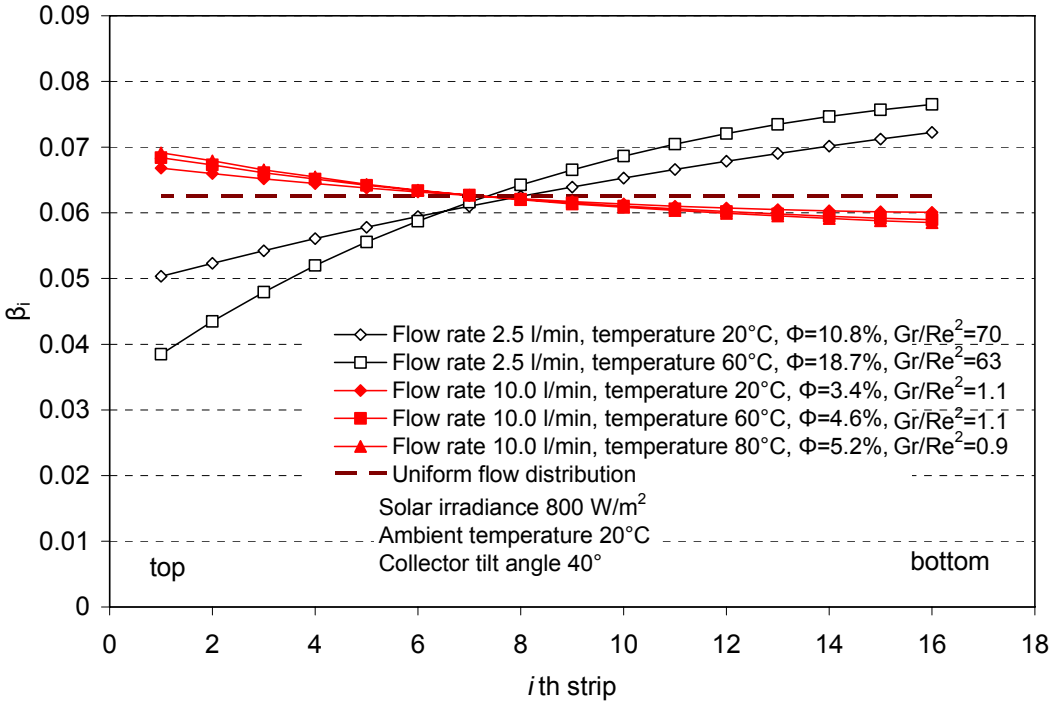

(A) Flow distribution

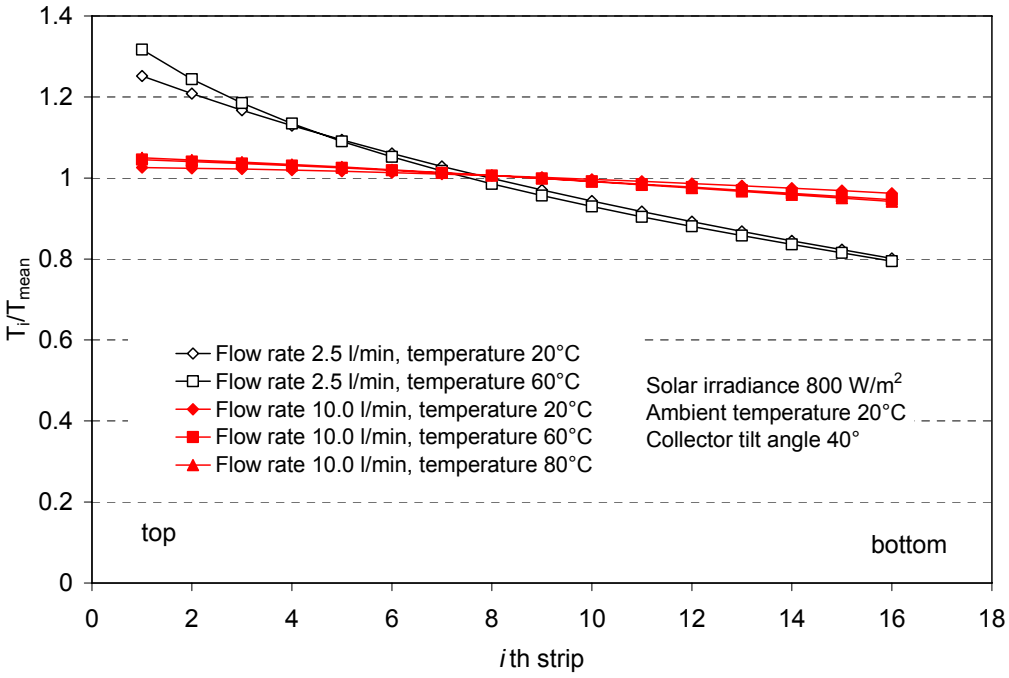

(B) Temperature distribution

Fig. 9: Volume flow rate and fluid temperature distributions in the strips for different solar collector fluid inlet temperatures.

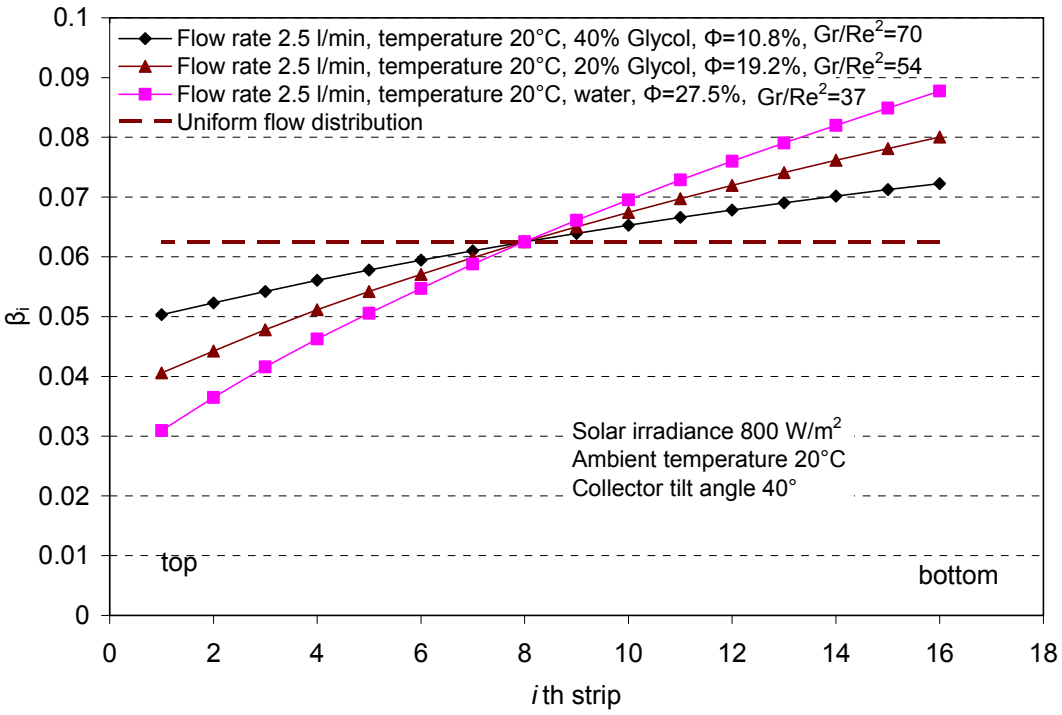

(A) Flow distribution

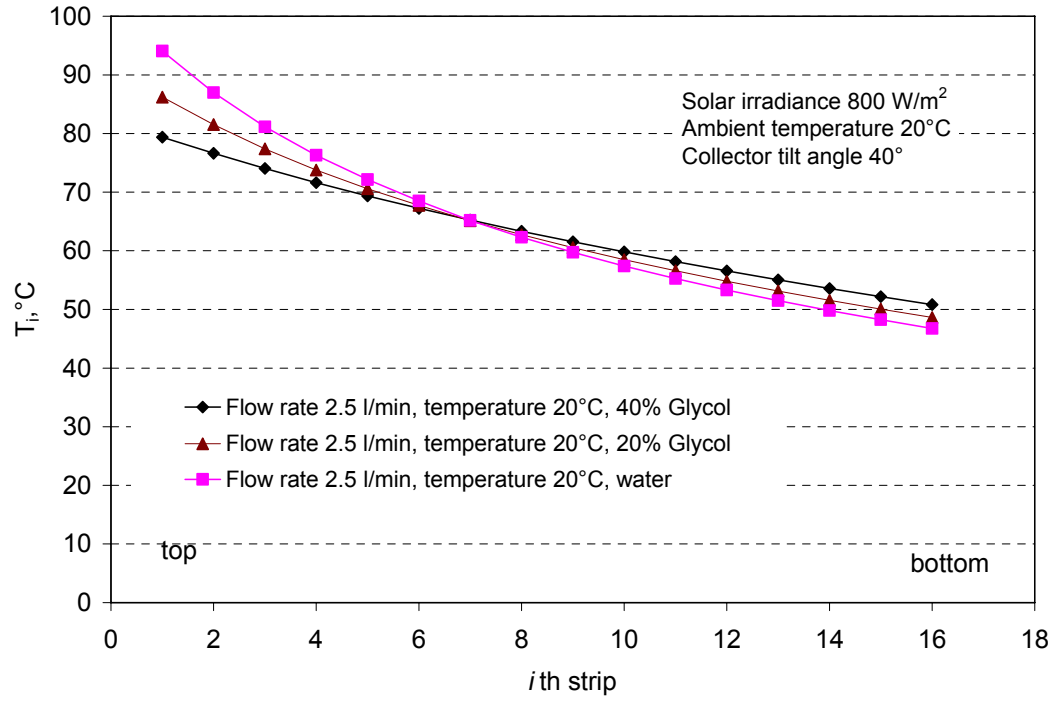

(B) Temperature distribution

Fig. 10: Volume flow rate and fluid temperature distributions in the strips for different solar collector fluids.

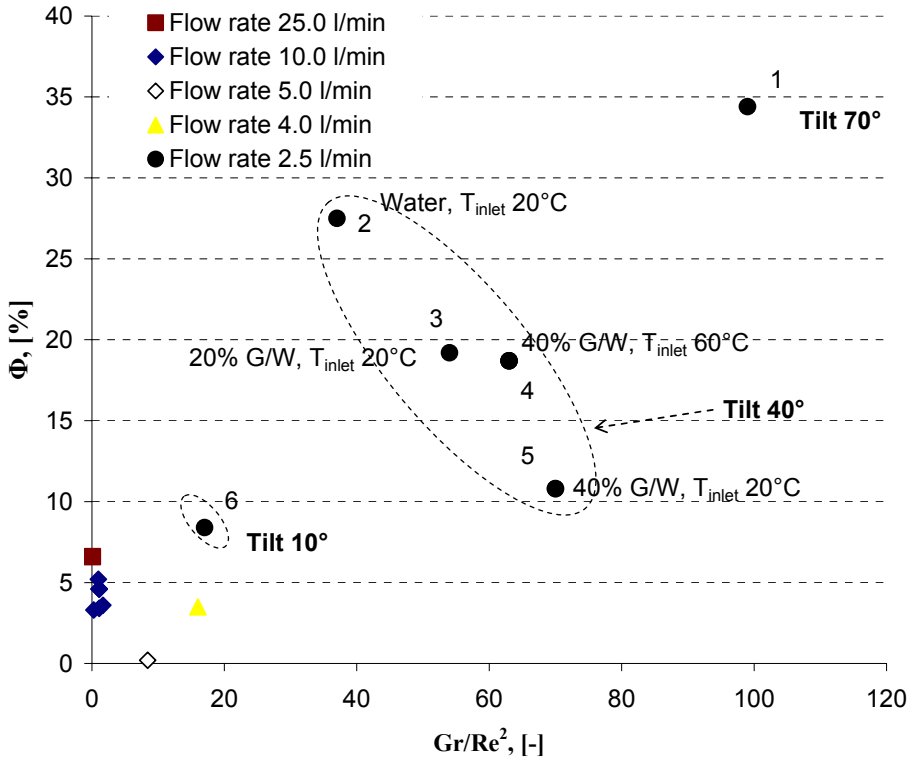

1 Glycol/water 40% , T_{inlet} 60°C, tilt 70°

2 Water, T_{inlet} 20°C, tilt 40°

3 Glycol/water 20% , T_{inlet} 20°C, tilt 40°

4 Glycol/water 40% , T_{inlet} 60°C, tilt 40°

5 Glycol/water 40% , T_{inlet} 20°C, tilt 40°

6 Glycol/water 40% , T_{inlet} 60°C, tilt 10°

Fig. 11: Plot of flow nonuniformity parameter Φ (%) of the U type collector versus Gr/Re^2 for different solar collector volume flow rates.